Science of the Total Environment 828 (2022) 154537

Contents lists available at ScienceDirect

Science of the Total Environment

journal homepage: www.elsevier.com/locate/scitotenv

Carbon-sulfur coupling in a seasonally hypoxic, high-sulfate reservoir in SW China: Evidence from stable CS isotopes and sulfate-reducing bacteria

Mengdi Yang [a], Cong-Qiang Liu [a,b], Xiao-Dong Li [a,b,*], Shiyuan Ding [a,d], Gaoyang Cui [c], Hui Henry Teng [a], Hong Lv [a], Yiyao Wang [a], Xuecheng Zhang [a], Tianhao Guan [a]

[a] Institute of Surface-Earth System Science, School of Earth System Science, Tianjin University, Tianjin 300072, China
[b] Tianjin Key Laboratory of Earth's Critical Zone Science and Sustainable Development in Bohai Rim, Tianjin University, Tianjin 300072, China
[c] Key Laboratory of Geospatial Technology for the Middle and Lower Yellow River Regions, Ministry of Education, College of Environment and Planning, Henan University, Kaifeng 475004, China
[d] State Key Laboratory of Environmental Geochemistry, Guiyang 550081, China

HIGHLIGHTS

- Carbon-sulfur coupling cycle was enhanced in hypoxic environment.
- SRB diversity determined the S isotope fractionation ($\Delta^{34}S$).
- High RWCS in July favored co-existence of complete-oxidizing and incomplete-oxidizing SRB.
- OC availability and composition affected $\Delta^{34}S$ via regulating SRB diversity.

GRAPHICAL ABSTRACT

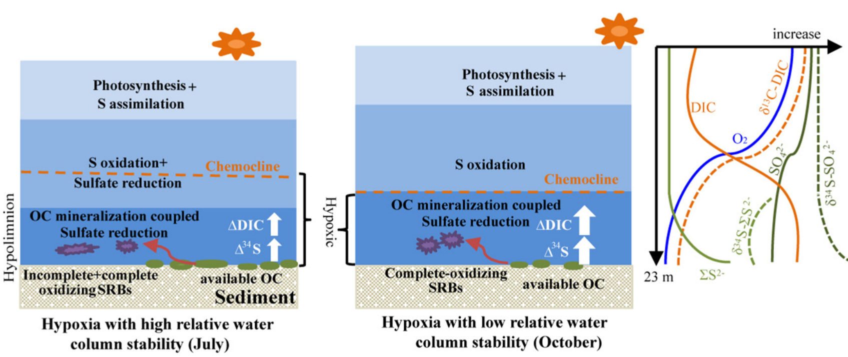

ARTICLE INFO

Article history:
Received 29 January 2022
Received in revised form 8 March 2022
Accepted 8 March 2022
Available online 12 March 2022

Editor: Xinbin Feng

Keywords:
Seasonal hypoxic reservoir
Sulfate reduction
Sulfur isotope fractionation
OC mineralization
Sulfate-reducing bacteria

ABSTRACT

Anthropogenic input of sulfate (SO_4^{2-}) in reservoirs may enhance bacterial sulfate reduction (BSR) under seasonally hypoxic conditions in the water column. However, factors that control BSR and its coupling to organic carbon (OC) mineralization in seasonally hypoxic reservoirs remain unclear. The present study elucidates the coupling processes by analyzing the concentrations and isotopic composition of dissolved inorganic carbon (DIC) and sulfur (SO_4^{2-}, sulfide) species, and the microbial community in water of the Aha reservoir, SW China, which has high SO_4^{2-} concentration due to the inputs from acid mine drainage about twenty years ago. The water column at two sites in July and October revealed significant thermal stratification. In the hypoxic bottom water, the $\delta^{13}C$-DIC decreased while the $\delta^{34}S$-SO_4^{2-} increased, implying organic carbon mineralization due to BSR. The magnitude of S isotope fractionation ($\Delta^{34}S$, obtained from $\delta^{34}S_{sulfate}$-$\delta^{34}S_{sulfide}$) during the process of BSR fell in the range of 3.4‰ to 27.0‰ in July and 21.6‰ to 31.8‰ in October, suggesting a change in the community of sulfate-reducing bacteria (SRB). The relatively low water column stability in October compared to that in July weakened the difference of water chemistry and ultimately affected the SRB diversity. The production of DIC (ΔDIC) scaled a strong positive relationship with the $\Delta^{34}S$ in July ($p < 0.01$), indicating that high OC availability favored the survival of incomplete oxidizers of SRB. However, in October, $\Delta^{13}C$-DIC was correlated with the $\Delta^{34}S$ in the bottom hypoxic water ($p < 0.01$), implying that newly degraded OC depleted in ^{13}C could favor the dominance of complete oxidizers of SRB which caused greater S isotope fractionation. Moreover, the sulfide supplied by BSR might stimulate the reductive dissolution of Fe and Mn oxides (Fe(*O*)OH

* Corresponding author at: Institute of Surface-Earth System Science, School of Earth System Science, Tianjin University, Tianjin 300072, China.
E-mail address: xiaodong.li@tju.edu.cn (X.-D. Li).

http://dx.doi.org/10.1016/j.scitotenv.2022.154537

and MnO_2). The present study helps to understand the coupling of C and S in seasonally hypoxic reservoirs characterized by high SO_4^{2-} concentration.

1. Introduction

The occurrence of hypoxia is a widespread anthropogenic impact that affect estuaries, marine, and freshwater environments (Al-Raei et al., 2009; Diaz and Rosenberg, 2008; Winton et al., 2019). When oxygen (O_2) concentration is low, the oxidation of labile organic carbon (OC) is often coupled with the reduction of nitrate, sulfate (SO_4^{2-}), ferric iron-bearing minerals, and other oxidized metals, hence affecting the biogeochemical cycles of biogenic elements such as carbon (C), nitrogen (N), sulfur (S), and of relevant metals (see Table 1 for oxidation sequence and reaction formula of these terminal electron acceptors) (Borch et al., 2010; Zhang et al., 2018). Due to the higher energy yield, nitrate is often preferentially coupled with OC oxidation in natural fresh waters. In polluted water bodies, such as reservoirs affected by past acid mining drainage, SC coupling becomes the predominant process due to the high concentration of SO_4^{2-}. Sulfate reduction in almost all natural environments is due to sulfate-reducing bacteria (SRB). In fact, bacterial sulfate reduction (BSR) is dominated in main process in the anaerobic oxidation of sedimentary marine organic matter (OM) and might account for up to 50% of OM mineralization (decomposition of the chemical compounds in OM, by which the nutrients in those compounds are released in soluble inorganic forms) in most continental shelf sediments (Jørgensen, 1982; Zhang et al., 2017).

The present study explored the coupling of C and S in a seasonally hypoxic reservoir that had been subject to decades-long effect of coal mining. For permanently hypoxic environments, a plethora of studies have delineated the coupling relationship between OC mineralization and BSR (Niggemann et al., 2007; Stam et al., 2010). To summarize, (1) the nature of OM plays an important role in controlling microbial metabolism of SRBs in deep sediment cores in the saline, alkaline Lake Van (Glombitza et al., 2013); (2) in turn, the BSR process produced high levels of fluorescent dissolved OM in freshwater sediment slurries (Luek et al., 2017); (3) the high abundance of dissolved organic carbon (DOC) and SO_4^{2-} in wetlands promoted SO_4^{2-} reduction to reach the highest rates ever measured, resulting in a large fraction of OC mineralization (Dalcin Martins et al., 2017). For seasonally stratified reservoirs, the existing understanding may not be readily applicable because of the inhomogeneity and fluctuating redox conditions in water columns (Borch et al., 2010). In general, the variation of water column stability in different stratified periods will affect the water chemistry and the composition of the functional communities of phytoplankton and planktonic bacteria (Cui et al., 2021; Yang et al., 2020b). Moreover, the rate of sulfate reduction and degree of S isotope fractionation (Knossow et al., 2015), as well as the electron transfer processes of OC mineralization in different seasons could also vary (Fahrner et al., 2008). As such, it is safe to conclude that the variable coupling mechanism between BSR and OC mineralization at different periods of stratification remains to be clarified in seasonally stratified reservoirs.

The sulfur isotopic signature of SO_4^{2-} ($\delta^{34}S$-SO_4^{2-}) is widely used in tracing SO_4^{2-} sources and exploring S biogeochemical processes in rivers, reservoirs and wetlands (Cao et al., 2018; Lewicka-Szczebak et al., 2008; Li et al., 2011). The combination of the $\delta^{34}S$-SO_4^{2-} with the $\delta^{13}C$-DIC is a powerful tool to reveal the coupling cycles of CS in aquatic environments (Cui et al., 2020; Hosono et al., 2014). It is well-known that, when SO_4^{2-} is reduced to hydrogen sulfide (H_2S) in BSR, ^{34}S is discriminated against by microorganisms and ^{32}S is preferentially used, causing ^{34}S to be relatively depleted in the hydrogen sulfide product (Bradley et al., 2016; Wasmund et al., 2017). The resultant fractionation can be quantified by the S isotope difference ($\Delta^{34}S$, calculated from $\delta^{34}S$-SO_4^{2-} and $\delta^{34}S$-ΣS^{2-}) that has implication from both microbial biochemistry and environmental factors (Antler et al., 2019; Canfield, 2001; Jørgensen et al., 2019). Because different groups of sulfate reducers degrade OC to different end products, and may cause different S isotope fractionation (Bradley et al., 2016; Detmers et al., 2001; Hamilton et al., 2016), it is essential to relate stable CS isotopes to SRB diversity to identify the biological factors driving the freshwater S cycle and to determine the roles of these bacteria in the coupling of OC mineralization and BSR.

Over the last decades, SO_4^{2-} concentrations in freshwater have increased globally (Zak et al., 2021), and BSR has been a major process in which SO_4^{2-} participated as electron acceptor in hypoxic freshwaters (Holmer and Storkholm, 2001). The Aha Reservoir, located in Guiyang City, with high SO_4^{2-} concentrations due to surrounding coal mines, is a typical freshwater ecosystem of the temperate zone, which becomes hypoxic due to thermal stratification from May to September (Song et al., 2011). In the present study, we sampled and measured the concentrations and isotopic compositions of C- and S-bearing aqueous species during four different months (January, April, July, and October in 2018) in the Aha Reservoir to explore the seasonal variation in the CS coupling effects. The SRB community composition was analyzed in July and October when the bottom water was hypoxic. Findings of this work will help to better understand the coupling mechanism of C and S biogeochemical processes in seasonal hypoxic ecosystems and to better predict the evolution of water quality.

2. Materials and methods

2.1. Study area

The present study was carried out in the Aha Reservoir in Guiyang City, SW China, which has a characteristic subtropical humid, monsoon climate.

Table 1
Oxidation sequence, redox couple, oxidation state and reaction formula of important terminal electron acceptors.

Oxidation sequence	Redox couple	Oxidation state	Reaction with OC
1	O_2/H_2O	0/−2	$O_2 + CH_2O \rightarrow H_2O + CO_2$
2	NO_3^-/N_2	+5/0	$4/5NO_3^- + CH_2O + 4/5H^+ \rightarrow CO_2 + 2/5\ N_2 + 7/5\ H_2O$
3	MnO_2/Mn^{2+}	+4/+2	$2MnO_2 + CH_2O + 4H^+ \rightarrow 2Mn^{2+} + 3H_2O + CO_2$
4	SeO_4^{2-}/SeO_3^{2-}	+6/+4	$2SeO_4^{2-} + CH_2O \rightarrow 2SeO_3^{2-} + CO_2 + H_2O$
5	$H_2AsO_4^-/H_3AsO_3$	+5/+3	$2H_2AsO_4^- + CH_2O + 2H^+ \rightarrow 2H_3AsO_3 + CO_2 + H_2O$
6	NO_3^-/NH_4^+	+5/−3	$NO_3^- + 2CH_2O + 2H^+ \rightarrow NH_4^+ + H_2O + 2CO_2$
7	Fe^{3+}/Fe^{2+}	+3/+2	$4FeOOH + CH_2O + 8H^+ \rightarrow 4\ Fe^{2+} + 7H_2O + CO_2$
8	SO_4^{2-}/S^{2-}	+6/−2	$SO_4^{2-} + 2CH_2O \rightarrow 2HCO_3^- + H_2S$

The theoretical reaction formulas are taken from references (Canfield et al., 1993; Gorny et al., 2015; Nancharaiah and Lens, 2015).

Canfield DE, Jørgensen BB, Fossing H, Glud R, Gundersen J, Ramsing NB, et al. Pathways of organic carbon oxidation in three continental margin sediments. Marine Geology 1993; 113: 27–40.

Gorny J, Billon G, Lesven L, Dumoulin D, Madé B, Noiriel C. Arsenic behavior in river sediments under redox gradient: A review. Science of The Total Environment 2015; 505: 423–434.

Nancharaiah YV, Lens PNL. Ecology and Biotechnology of Selenium-Respiring Bacteria. Microbiology and Molecular Biology Reviews 2015; 79: 61–80.

The average annual temperature is 15 °C, with extreme temperatures of 35 °C in summer and −10 °C in winter (Wang et al., 2010). The wet season of the watershed usually begins from May and lasts till October every year, which accounts for about 75% of the total annual precipitation (1129.5 mm) (Li et al., 2014). Aha Reservoir is one of the many deep-water (>10 m) reservoirs where hypoxia occurs frequently in summer (Zhang et al., 2015). The upstream Aha Reservoir is mainly recharged by the Youyu River, which flows through dense coal mining area including the Dapo Coal Mine that produced a large amount of acidic runoff (~7000 m^3/year; pH < 3) with high concentrations of Fe (II) (~1 g L^{-1}) and SO_4^{2-} (~7 g L^{-1}) (Sun et al., 2015). The mine waste water discharged from the coal kilns and the rainwater that washes away the gangue leachate solution containing high levels of iron and manganese into the reservoir, causing a continuous accumulation of iron and manganese in the sediments at the bottom of the lake, which also leads to a high concentration of sulfate (up to 300 mg L^{-1}) in the water body (Song et al., 2011). Located in the downstream Aha reservoir, the Sha River has long been discharging domestic sewage with high OM content in the water body. High concentrations of SO_4^{2-}, Fe, and OC at the water-sediment interface and hence constitutes a fitting environment to study microbially-driven S cycling (Li et al., 2020; Sun et al., 2015). Although several studies have previously investigated the transformation of heavy metals (Ding et al., 2022; Feng et al., 2011), composition of phytoplankton community (Han et al., 2018), SO_4^{2-} cycling (Findlay et al., 2019; Song et al., 2011), and differences in microbial diversity in sediments subjected to different coal mine contamination gradients in Aha watershed (Sun et al., 2015), the influence of BSR processes on OC mineralization under seasonal hypoxia in SO_4^{2-}-rich water columns remain unclear until this study.

2.2. Sampling and analyses

2.2.1. Field sampling

In this study, two sampling sites (Zhongcaosi, Station ZCS; Nanjiao, Station NJ) of Aha reservoir were selected (Fig. 1). Samples of surface water were collected at 0.5 m below water surface, and samples of water column were taken using Niskin Water Sampler (General Oceanics, USA) according to the specific depths of the two sites (Table S1), during four seasons in January (winter), April (spring), July (summer), and October (autumn) 2018. Water temperature (T), pH, O_2 and Oxidation-Reduction Potential (ORP) were measured in situ with a pre-calibrated, automated multi-parameter profiler (model: YSI EXO-1). The total dissolved sulfide ($\Sigma S^{2-} = H_2S + S^{2-} + HS^-$) was measured in the field by the methylene blue method (Mylon and Benoit, 2001) using a portable spectrophotometer (DR1900, Hach, USA). The thermal stability of the water column can be efficiently assessed by the relative water column stability (RWCS, see below), which was defined as $(\rho_s - \rho_b)/(\rho_4 - \rho_5)$. The ρ_s and ρ_b are the density of surface and bottom water, respectively, in kg m^{-3}, while ρ_4 and ρ_5 are the pure water density at 4 °C and 5 °C, respectively. The water density is a function of water temperature (°C) and can be calculated from the empirical formula (1) (Lawson and Anderson, 2007):

$$\rho_T = 1000 \times \left[1 - \frac{(T + 288.9414) \times (T - 3.9863)^2}{508929.2 \times (T + 68.1296)}\right] \quad (1)$$

2.2.2. Pretreatment of samples

The water samples were filtered through 0.45 μm microporous nitrocellulose membrane (Millipore), and the 15-mL filtered samples were stored in clean centrifuge tubes at 4 °C for analyses of anions and cations. A few drops of twice-distilled nitric acid were added into other 15-mL filtered subsamples to make pH < 2 for heavy metals tests. For δ^{13}C-DIC analysis, the 2-mL samples filtered with 0.45-μm polytetrafluoroethylene syringe filters were injected into 10-mL LABCO vials under pre-treatment vacuum, and 1-mL phosphoric acid was added with a syringe. For $\delta^{34}S$-ΣS^{2-} analyses, the 5 L water samples were pretreated with 5% ascorbic acid and 30 wt% zinc acetate, the ZnS produced was then transformed to Ag_2S by adding phosphoric acid with silver nitrate (Geng et al., 2018). Detailed steps of the Ag_2S preparation from ZnS and details about its variations of isotope composition in the process are shown in Supplementary S1. The filtered

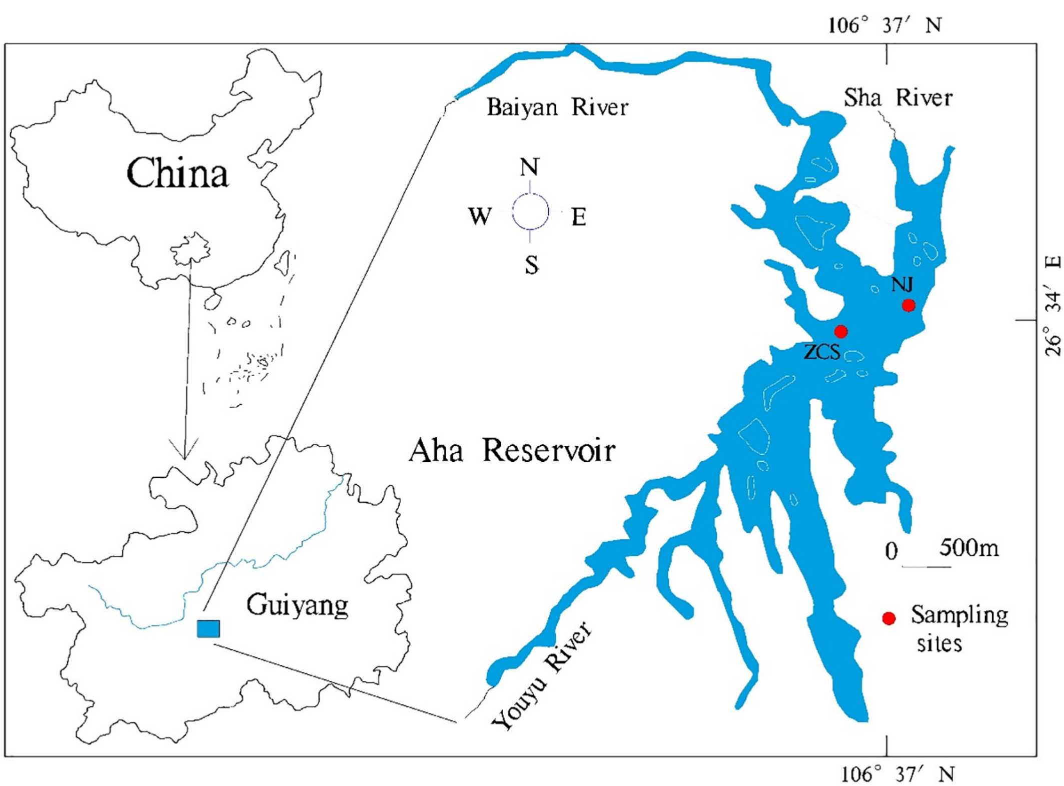

Fig. 1. Map of Sampling sites in Aha reservoir. Location of the two sampling sites in the Aha reservoir: Zhong Caosi (ZCS) and Nan Jiao (NJ).

samples for δ^{34}S-SO_4^{2-} measurements were acidified to pH < 2 with concentrated HCl before the SO_4^{2-} was precipitated as $BaSO_4$ with excess $BaCl_2$. Bacterioplankton was collected on 0.22 μm sterilized membrane filters (MF-Millipore, USA) using a vacuum pump, and then stored at −20 °C until DNA extraction.

2.2.3. Chemical and isotopic analyses

The dissolved inorganic carbon (DIC) was calculated from pH and alkalinity, which was determined by titrating with 0.02 mol L^{-1} hydrochloric acid within 8 h after sampling. The concentration of DOC was determined on an Aurora 1030 total OC analyzer (OI Analytical) with duplicates (± 1.5%, analytical error). The SO_4^{2-} anion was analyzed by ion chromatography ICS-5000+ (Thermo Fisher). The heavy metals (Fe and Mn) were measured by inductively coupled plasma mass spectrometer (ICP-MS) (Agilent, 8900). The δ^{34}S-SO_4^{2-} and δ^{34}S-ΣS^{2-} were measured by isotope ratio mass spectrometer (IRMS, Delta V advantage, Thermo Fisher) interfaced with an elemental analyzer (Flash 2000HT). The δ^{13}C-DIC was measured by a GasBench II device interfaced with a Delta V Plus instrument (Thermo Fisher). Isotopic ratios are expressed in terms of δ notations (‰) relative to the Vienna Canyon Diablo Troilite (V-CDT) standard for S and Vienna Pee Dee Belemnite (V-PDB) (%) standard for C. The overall analytical accuracy for δ^{13}C measurements was 0.3‰, as calibrated by the standard NBS-18. The overall experimental accuracy of δ^{34}S-SO_4^{2-} and δ^{34}S-ΣS^{2-} were estimated to better than 0.2‰ based on standards NBS-127, IAEA-S-1 and IAEA-SO-6.

2.2.4. DNA extraction, PCR amplification, sequencing and data processing

For DNA extraction, genomic DNA was extracted in duplicate using the Fast DNA® SPIN Kit for Soil (MP Biomedicals, USA). The duplicate DNA extracts were finally mixed for the following PCR amplification. The V3-V4 region of the bacterial 16S ribosomal RNA gene was amplified by PCR using barcoded primers 338f/806r (Tong et al., 2018). Purified amplicons were pooled in equimolar amounts and sequenced using the strategies of PE250 (paired-end sequenced 250 × 2) on an Illumina MiSeq platform (Majorbio Company in Shanghai).

Operational taxonomic units (OTUs) were clustered with 97% similarity cutoff using UPARSE(version 7.1 http://drive5.com/uparse/). The taxonomy of each 16S rRNA gene sequence was analyzed by RDP Classifier algorithm (http://rdp.cme.msu.edu/) against the Silva (SSU132) 16S rRNA database using a confidence threshold of 70%. The detailed condition of PCR amplification and reactions, as well as the treatment of raw fastq files, are shown in Supplementary Section S2. The raw sequence data have been deposited in the NCBI Sequence Read Achieve (SRA) under accession number SRP321486.

3. Results

3.1. Seasonal thermal stratification

3.1.1. Water chemistry

T, pH and O_2 in the water column remained basically unchanged with depth in January at both Station ZCS and Station NJ (Figs. 2a and S2a). T, pH and O_2 decreased from the surface water to 8 m-depth water in April, but were nearly unchanged from 8 m-depth to the deepest 20 m (Figs. 2b and S2b), because the water body started to stratify in April. Specifically, O_2 reached a maximum of 13.70 mg L^{-1} in the surface water and a minimum of 0.79 mg L^{-1} in the bottom water in April, indicating strong photosynthesis in the surface water column and anaerobic decomposition of OM in the bottom water. The differences of T, pH and O_2 between surface water and bottom water were particularly pronounced in July (Figs. 2c and S2c) due to strong thermal stratification which caused hypoxia below 8 m. In October, the depth differences of physicochemical parameters in the water column became smaller (Figs. 2d and S2d), though the stratification still existed. Sulfide concentrations in January and April were below detection, however, sulfide was generated (>1 μM) in the hypoxic water at 12 m in July and at 16 m in October (Table 2), and trended upward into the deepest water (Fig. 3). Seasonally, thermal stratification existed in April, July and October. The hypoxia induced by O_2 depletion and sulfide production also exhibited seasonality, which was related to intense stratification in July and October.

3.1.2. Relative water column stability (RWCS)

The RWCS is a dimensionless parameter that can be used to describe the thermal stratification and water vertical mixing. The greater the RSCW, the stronger the thermal stratification (Becker et al., 2008). The RWCS showed no significant differences between ZCS and NJ water columns in the same season but varied seasonally according to the thermal stratification, with the highest value in July (400.8 at ZCS) and the lowest value in January (3.6 at ZCS) (Table S2). Although July and October were both in the stratification period according to the RWCS, there were differences in the depth of the chemocline (which is defined here as the shallowest depth with sulfide concentration above 1 μM) in July and October. In July, the chemocline depth was at 12 m, while it moved down in October to 16 m. The water depleted in O_2 below the chemocline is defined as hypolimnion.

3.2. Sulfur speciation and isotopic composition

In January, no significant depth variations of SO_4^{2-} concentration and δ^{34}S-SO_4^{2-} in the water columns were observed. However, in April, the SO_4^{2-} concentration decreased with depth, accompanied by a small increase in δ^{34}S-SO_4^{2-}, from −7.82‰ at the surface water to −7.44‰ at 8 m at Station ZCS (Fig.S2). In July, the SO_4^{2-} concentration ranged between 1.34 and 1.88 mmol L^{-1} with a mean value of 1.60 mmol L^{-1}. Below 18 m, ΣS^{2-} sharply increased up to 0.10 mmol L^{-1} at 20 m (Fig. 3a). The δ^{34}S-SO_4^{2-} ranged between −8.4‰ and − 4.3‰ with an average of −6.1‰, and decreased from −4.95‰ in the surface water to −7.90‰ at 12 m then trended upward from −8.40‰ at 16 m to −5.75‰ near the bottom at 20 m at Station ZCS. The δ^{34}S-ΣS^{2-} decreased from 12 m to 19 m. In October, water depths at ZCS and NJ increased to 22 m and 23 m, respectively. Similar to July, ΣS^{2-} was generated and sharply increased below 16 m to 0.13 mmol L^{-1} at 22 m at ZCS and 0.22 mmol L^{-1} at 23 m at NJ (Fig. 3b). However, the ΣS^{2-} concentration decreased sharply and the SO_4^{2-} concentration shifted upward, together with the δ^{34}S-SO_4^{2-}decreased from −2.40‰ to −4.95‰ within the lowest 1 m above sediment of NJ in October. The δ^{34}S-SO_4^{2-} values increased slightly from the surface −8.63‰ to −8.48‰ at 12 m, showed a slight minimum of −9.83‰ at 16 m, and then increased from 16 m to the bottom at Station ZCS. The δ^{34}S-ΣS^{2-} first decreased at 16–18 m and then increased with depth, both at Station ZCS and NJ.

3.3. Spatiotemporal variations of DIC and δ^{13}C-DIC

Both DIC concentration and δ^{13}C-DIC presented significant seasonal variations in the water columns, and interestingly they showed different trends in all four seasons except for winter (January) (Fig. 4). Overall, DIC concentrations ranged from 2.92 ± 0.07 mmol L^{-1} in January, 2.59 ± 0.49 mmol L^{-1} in April, 2.80 ± 0.71 mmol L^{-1} in July and 3.34 ± 0.66 mmol L^{-1} in October. The δ^{13}C-DIC varied with the season from −8.3‰ ± 0.4‰ in January, 6.5 ± 3.0‰ in April, 9.1 ± 2.8‰ in July and 9.3 ± 2.2‰ in October. In April, July and October, DIC concentration increased with depth while the δ^{13}C-DIC concurrently decreased from the surface to 12 m. The increase in DIC and decrease δ^{13}C-DIC were steeper from 12 m to the bottom water. In April, July and October, above 12 m, photosynthesis by phytoplankton was utilized the DIC in the uppermost water column, while anaerobic decomposition of OM under hypoxic conditions produced DIC below 12 m (Fig. 4).

3.4. Taxonomy and seasonal dynamics

The 16S rRNA sequencing analyses revealed that bacteria in the water body consist of 3672 Operational Taxonomic Units (OTUs) from 1755

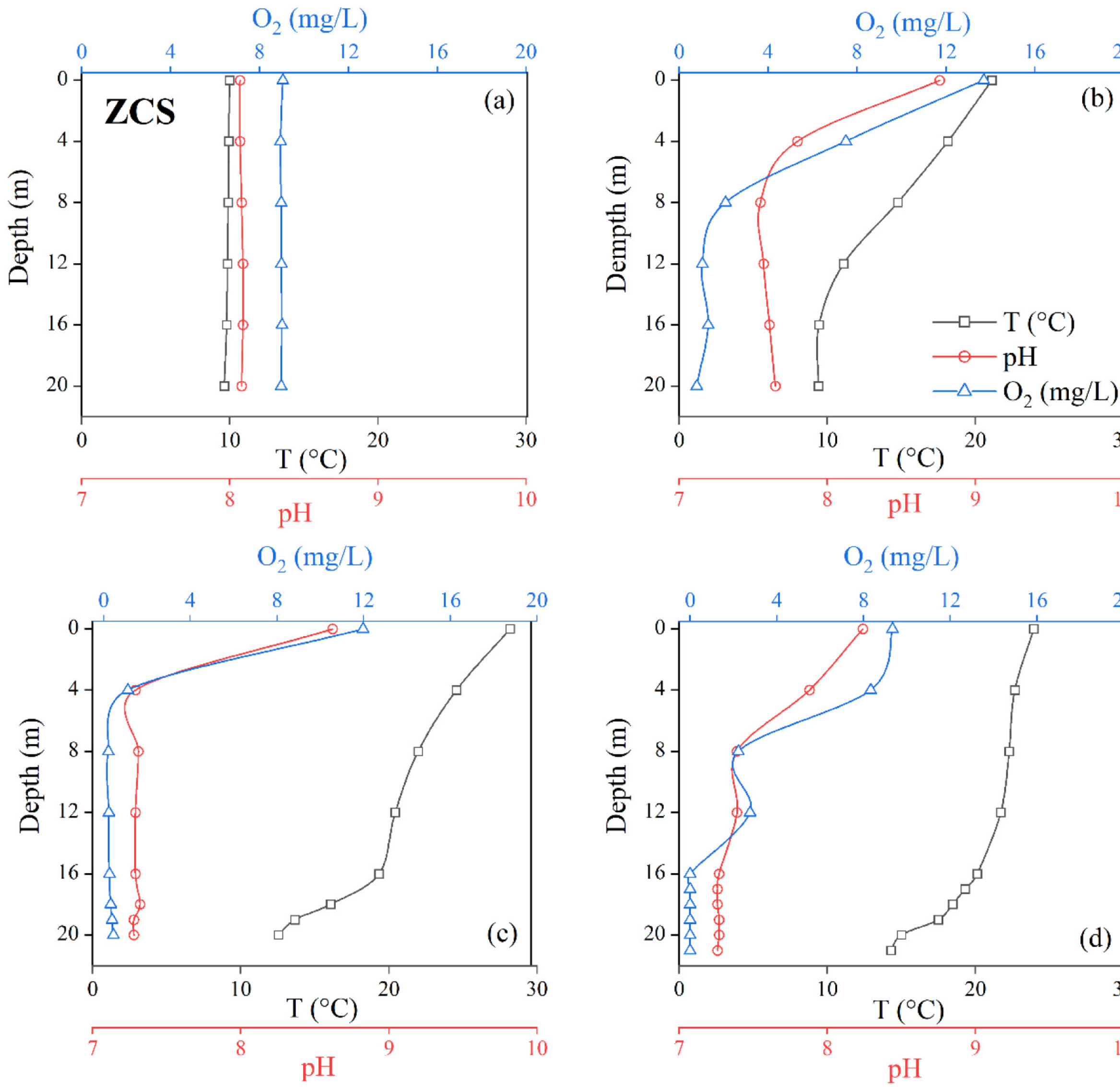

Fig. 2. Spatiotemporal variations of temperature (T), pH and oxygen (O_2). (a) is for January, (b) is for April, (c) is for July and (d) is for October. The value of the data (T, pH and O_2) in the ZCS water column were used to draw the graph. The spatiotemporal variations of these data in NJ showed similar trends as ZCS, which were showed in Fig.S1.

species, 986 genera, 551 families, 327 orders, 141 classes, and 48 phyla. Among these, a total of 124 OTUs were identified as belonging to potential SRB, based on family classification of the OTUs. Furthermore, these SRB OTUs were affiliated with 20 families, accounting for 0.00–5.40% (0.83% on average) of the total 16S rRNA gene sequences. Moreover, this ratio of SRB OTUs showed increasing trends from surface water to bottom water in July and October (Table S3). Seasonally, significant differences were found in SRBs at the genus level (Fig. 5): *Desulfatirhabdium; norank_f_Desulfobacteraceae*; *Desulfobacterium_catecholicum_group; Desulfovibrio* were dominant in July, while *Desulfatirhabdium*, *Desulfomonile, and Desulfatiglans* dominated in October. Moreover, the proportions of different main SRBs were more uniform in July, while *Desulfatirhabdium* and *Desulfomonile* were predominant in October.

4. Discussion

4.1. S biogeochemical processes in the water column

The residence time of water in the studied reservoir is approximately half a year (Song et al., 2011), and the reservoir is seasonally stratified during the summer and into the autumn, with stable stratification from July to October, and mixes during the winter and spring. This yearly stratification cycle combined with the relatively short residence time means that the physical and chemical conditions of the water column change on seasonal time scales (Yang et al., 2020a). Despite this variability, the water column is at quasi-steady-state during stratification, meaning that the biogeochemical processes occur faster than the horizontal mixing processes (Findlay et al., 2019). This in turn means that the concentration and isotopic composition of S species in the water column are affected by and show the signatures of in situ biogeochemical processes, such as BSR (Findlay et al., 2019; Song et al., 2011).

In January, the water column was well mixed and aerobic, the low plankton growth in surface water caused little S assimilation, and sulfate reduction was inhibited in the aerobic water column (Knossow et al., 2015). Compared to January, the 0–8 m water column in April had lower concentrations of SO_4^{2-} that was relatively enriched in ^{34}S, revealing that S assimilation possibly occurred from surface water to 8 m in Station ZCS in April (Fig. S2). Concentrations of chlorophyll *a* were particularly high in the surface waters in April (Fig.S3). Chlorophyll *a* concentration is a measure of phytoplankton biomass across a broad trophic gradient of lakes (oligotrophic–highly eutrophic) and has a highly significant positive correlation with phytoplankton biomass (Desortová, 1981; Kasprzak et al., 2008).

Table 2
The concentrations and sulfur isotopic values of sulfate and sulfide and S isotope difference between sulfate and sulfide of BSR in the studied water column of Aha Reservoir.

	Site-depth	$\delta^{34}S$-SO_4^{2-} (‰)	$\delta^{34}S$-ΣS^{2-} (‰)	SO_4^{2-} (mmol L^{-1})	S^{2-} (μmol L^{-1})	$\Delta^{34}S$ (‰)	*f* (%)
July	Z-12	−7.90	−11.30	1.69	1.31	3.40	0.08%
	Z-16	−8.40	−16.49	1.43	1.75	8.09	0.12%
	Z-18	−6.98	−18.32	1.86	3.38	11.34	0.18%
	Z-19	−5.43	−32.38	1.88	99.84	26.95	5.03%
	Z-20	−5.75	−31.91	1.84	113.59	26.16	5.81%
	N-16	−6.19	−12.98	1.44	1.50	6.78	0.10%
	N-18	−7.11	−22.10	1.58	3.75	14.99	0.24%
	N-19	−6.62	−30.94	1.75	72.19	24.32	3.96%
	N-20	−5.29	−28.51	1.82	83.70	23.23	4.40%
October	Z-17	−9.21	−36.84	1.87	1.63	27.62	0.09%
	Z-18	−9.14	−40.91	1.88	15.63	31.77	0.82%
	Z-19	−7.64	−37.92	1.73	46.41	30.28	2.61%
	Z-20	−5.24	−36.50	1.62	96.88	31.26	5.64%
	Z-21	−2.51	−34.05	1.56	135.78	31.54	7.99%
	Z-22	−1.82	−32.01	1.33	95.63	30.19	6.72%
	N-17	−8.07	−32.54	1.61	19.25	24.47	1.18%
	N-18	−8.12	−33.66	1.64	26.72	25.55	1.61%
	N-19	−7.55	−35.36	1.64	52.81	27.81	3.13%
	N-20	−5.87	−34.55	1.61	105.19	28.67	6.13%
	N-21	−3.88	−31.24	1.54	125.00	27.36	7.52%
	N-22	−2.40	−29.97	1.50	220.00	27.58	12.81%
	N-23	−4.95	−26.59	1.54	1.38	21.64	0.09%

In the table, the $\Delta^{34}S$ is S isotope difference between sulfate and sulfide, *f* is the ratio of sulfide to sulfate plus sulfide.

Phytoplankton in the surface water grew rapidly and favored S assimilation with increasing temperature in April (Wang, 2020). Although the stratification began in April and the O_2 concentration in the bottom water was low (Fig. 2), the BSR might still have been limited due to lack of available OC from the spring phytoplankton production (Kwon et al., 2016).

In July, from 0 m to 12 m, similar to April, S assimilation or S oxidation may occur in the surface oxygenated water column with high chlorophyll *a*. From July to October, the surface water column may be affected by rainfall, which may also have an impact on SO_4^{2-} concentrations and $\delta^{34}S$-SO_4^{2-}. From a depth of 12 m downwards, SO_4^{2-} reduction begins to take place, as evidenced by the increase of ΣS^{2-} concentration as well as the depletion of O_2. From 12 to 16 m, the concurrent decrease in SO_4^{2-} concentration and relatively constant $\delta^{34}S$-SO_4^{2-} indicate that sulfate reduction and S oxidation may have proceeded simultaneously. Nitrate was probably the main oxidizing agent (unpublished data). The BSR consumed SO_4^{2-} and resulted in ^{34}S enrichment in the residual SO_4^{2-} below the chemocline. Below 16 m, the ΣS^{2-} increased sharply together with an increase of $\delta^{34}S$-SO_4^{2-} with depth (Fig. 3a), revealing the enhancement of BSR in the hypoxic water with depleted O_2 and a large community of SRBs (Fig. 2 and Table S3).

In October, an increase in SO_4^{2-} concentration can be seen at 12 m to 16 m where S oxidation took place (Fig. 3b). Reduced sulfur in metal sulfides in suspended particulate matter is anaerobically oxidized by nitrate reducing bacteria to produce SO_4^{2-} (Zhang et al., 2022). Below 16 m, the ΣS^{2-} sharply increased with depth together with an increase of $\delta^{34}S$-SO_4^{2-}, showing that BSR occurred in the hypoxic water below chemocline (Fig. 3b). The increasing ΣS^{2-} with depth was accompanied by an increase in the relative proportion of SRB both in July and October, showing the coupling of the sulfate reduction process and an increasing relative abundance of SRB (Table S3).

Sulfide re-oxidation occurred just above the sediment-water interface of ZCS in October (Fig. 3b). In this study, the concentrations of Fe and Mn showed notable changes. Both Fe and Mn increased significantly in the hypoxic bottom water in July and October (Fig. S4). The dissolved Mn and Fe were positively correlated with ΣS^{2-} (Fig. S5), and Mn (IV) and Fe (III) in the sediment oxidized sulfide in the overlying water (Fig. 3b). Recent studies have shown that sulfide produced through sulfate reduction can first react with Mn oxide to produce elemental sulfur and finally produce SO_4^{2-} in sulfate-poor, non-marine environments during early diagenesis (Cai et al., 2021). As the sediments were also in the hypoxic environment, iron and manganese oxides, formed during the period of water mixing in winter, were the main oxidants of sulfide during the stratified period (Findlay et al., 2019). The decrease in $\delta^{34}S$-SO_4^{2-} near the sediment was also evidence for the occurrence of sulfide re-oxidation. However, the water samples taken in July did not fully reach the water-sediment interface, so no significant evidence for sulfide re-oxidation was observed.

The density difference between warm surface waters and the colder bottom water prevented the reservoir water from mixing in July and October (Xing et al., 2019). The resultant stratification and bottom hypoxia in July and October were favorable for the growth of SRB and the occurrence of BSR (Mori et al., 2018). According to Eq. (2), the BSR consumed OC and SO_4^{2-} to generate DIC and sulfide:

$$2CH_2O + SO_4^{2-} \rightarrow 2HCO_3^- + H_2S \quad (2)$$

Since the concentrations of S intermediates ($S_0 < 3$ μM, $S_2O_3^{2-} < 1$ μM, $SO_3^{2-} < 1$ μM) in Aha reservoir were extremely low (Findlay et al., 2019), the ratio of sulfide to SO_4^{2-} plus sulfide ($f = \Sigma S^{2-} / (SO_4^{2-} + \Sigma S^{2-})$) could be used to represent the degree of SO_4^{2-} reduction. Seasonally, *f* increased with depth both in ZCS and NJ water column hypolimnion. However, *f* in October was much higher than that in July (Table 2), implying higher degree of sulfate reduction in October. The apparently lower SO_4^{2-} concentration in the hypolimnion in October than in July was also strong evidence, because more SO_4^{2-} was consumed in October in the absence of a deep-water SO_4^{2-} supply. Similar results were found in the water column of Lake Kinneret in Israel where BSR occurred between May and October and the maximum ΣS^{2-} existed in October because the continuous accumulation of hypolimnetic sulfide as the result of BSR was supported by a high influx of OM (Knossow et al., 2015).

4.2. S isotope fractionation

4.2.1. SO_4^{2-}-sulfide fractionation ($\Delta^{34}S$)

As described above, the BSR process occurred in the hypoxic bottom water in July and October. Generally, the BSR will cause a S isotope fractionation in SO_4^{2-}, and the magnitude of isotope fractionation can be described by the difference between SO_4^{2-} and sulfide fractionation as Eq. (3) (Findlay et al., 2019; Jørgensen et al., 2019):

$$\Delta^{34}S = \delta^{34}S_{sulfate} - \delta^{34}S_{sulfide} \quad (3)$$

In Aha reservoir, $\Delta^{34}S$ increased with depth from 3.4‰ to 27.0‰ in July, while it was between 21.6‰ and 31.8‰ in October (Fig. 6). These results are consistent with the previous findings in bottom water and pore

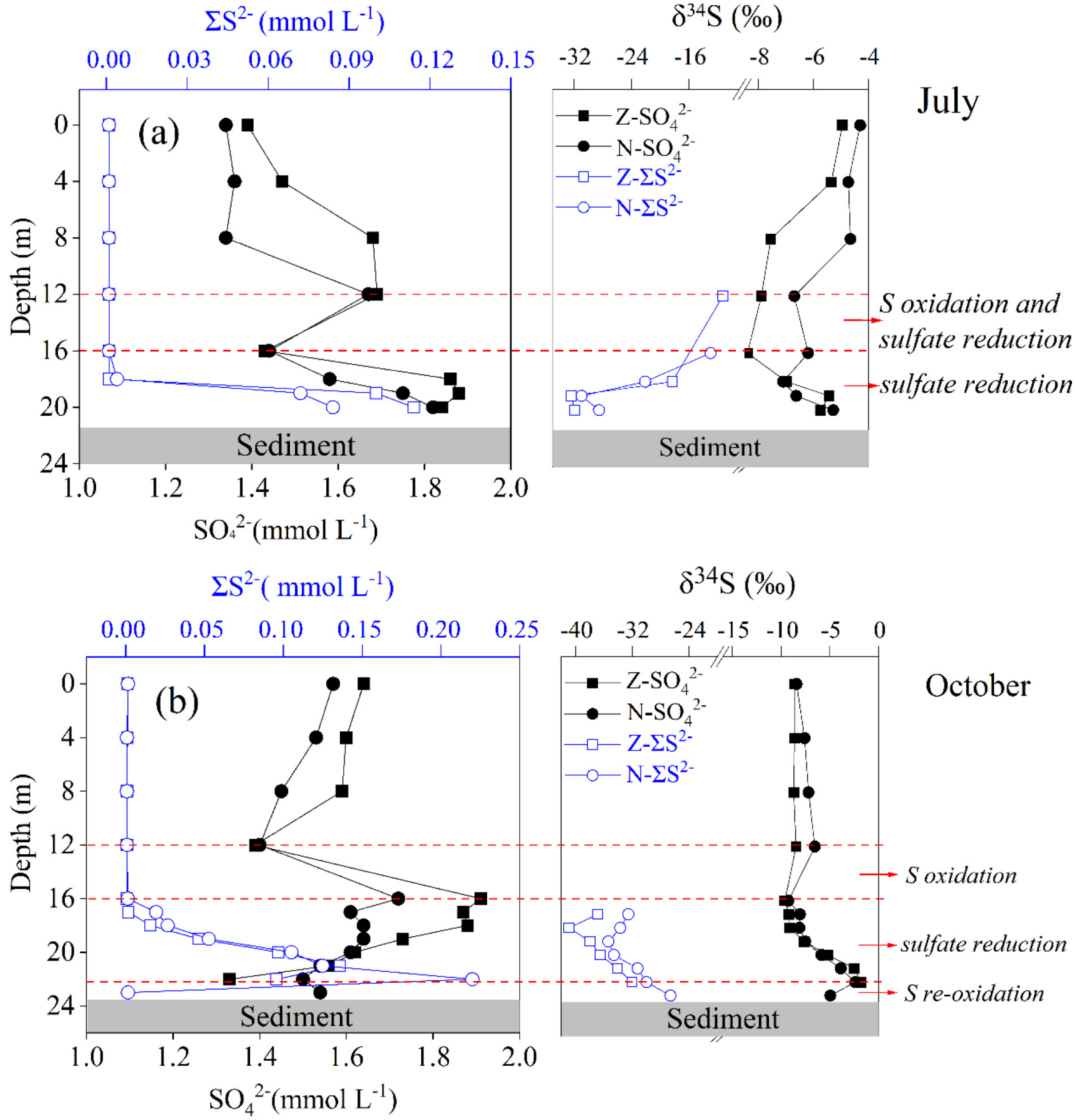

Fig. 3. Spatiotemporal variations of concentration and isotopic composition of sulfate and sulfide at stations ZCS (Z) and NJ (N) in July and October. The predominant sulfur reactions are indicated.

water of Aha reservoir, where the $\Delta^{34}S_{sulfate\text{-}sulfide}$ was between 17‰ and 30‰ in August (Findlay et al., 2019), and was in the range of experimental fractionation factors from 2.0‰ to 42.0‰ in laboratory incubation experiments (Detmers et al., 2001). The SO_4^{2-} concentration was not the determining factor for $\Delta^{34}S$ in the study area because it kept at a high concentration (>1 mmol L^{-1}) for all samples (Fig. 3).

4.2.2. Influencing factors

The seasonal variations of $\Delta^{34}S$ in the two monitored water columns were similar; however, the $\Delta^{34}S$ showed increasing trend with depth in July, while the $\Delta^{34}S$ was more stable and larger in October (Fig. 6). The increasing trend of $\Delta^{34}S$ with depth in July may be due to different types of SRB that grew at different depths. Genetic and physiological differences between genera of SRB affect the isotopic fractionation. Complete oxidizers (SRB that oxidize OC completely to CO_2) tend to cause greater isotope fractionation than incomplete oxidizers (SRB that oxidize OC incompletely to acetate or other products) (Detmers et al., 2001; Hamilton et al., 2016). The higher relative abundance of incomplete oxidizers (such as *Desulfovibrio* and *Desulfomicrobium)* in the hypolimnion in July (Fig. 5) resulted in an overall smaller $\Delta^{34}S$. The relative abundance of dominant complete oxidizers showed an increase trend in July with depth increase in the hypolimnion (Fig. 5), resulting in an increase in the $\Delta^{34}S$ with depth. While in October, the nearly unchanged but greater $\Delta^{34}S$ (with an average of 29.1‰) revealed predominant survival of complete-oxidizing sulfate reducers (as *Desulfatirhabdium*, *Desulfomonile)* and no significant variations of complete-oxidizing sulfate reducers with depth (Detmers et al., 2001; Knossow et al., 2015).

The SRB community changed with varying T, pH and O_2 in the water column, as the growth of SRB was sensitive to these environmental changes (Kushkevych et al., 2019; Mori et al., 2018; Robador et al., 2009). Therefore, environmental factors, including T, O_2 concentration, substrate type, OC availability, and SO_4^{2-} concentration, may also play important roles in the magnitude of $\Delta^{34}S$ (Bradley et al., 2016; Jørgensen et al., 2019; Kleikemper et al., 2004). Based upon a redundancy analysis (RDA;

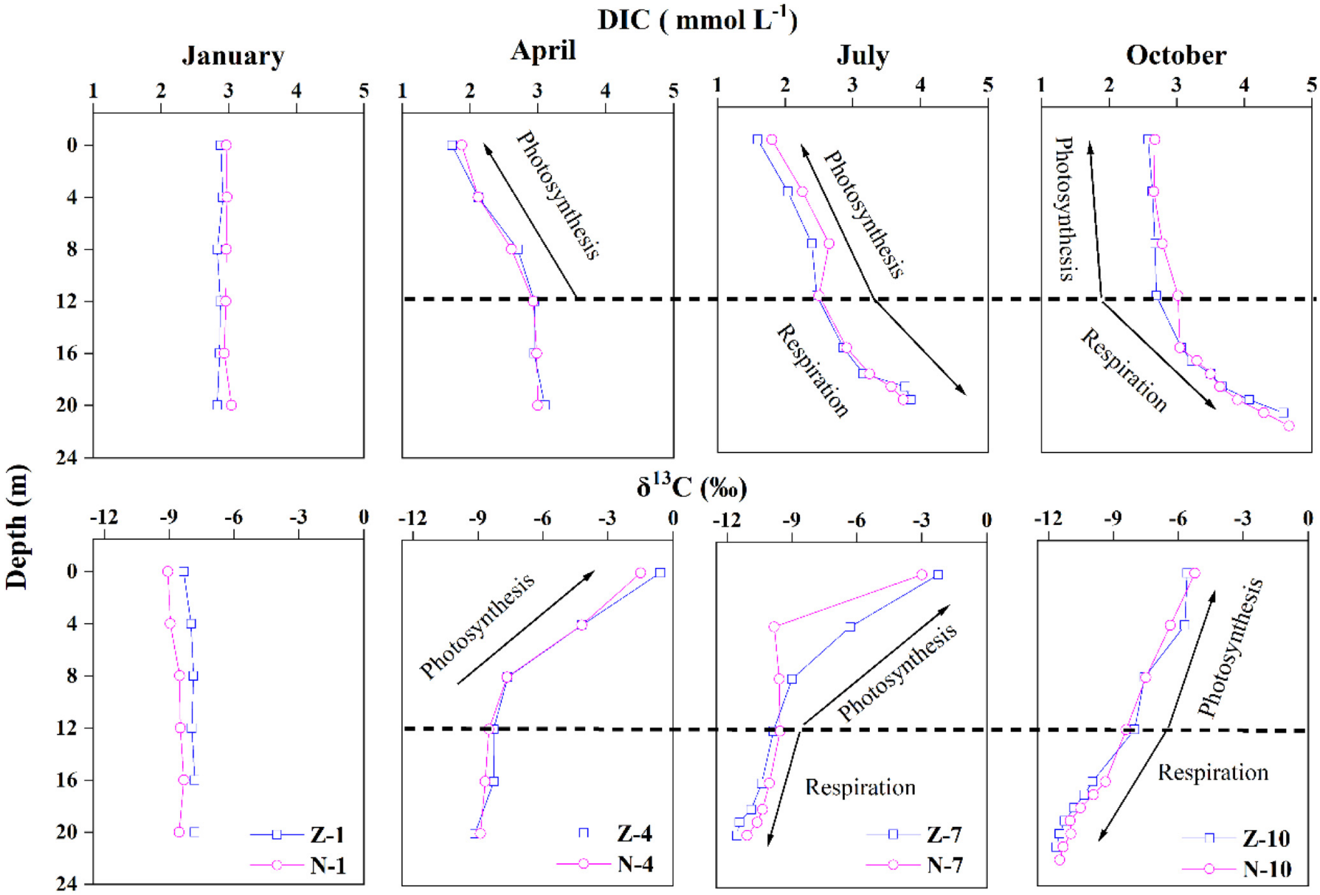

Fig. 4. Spatiotemporal variations of DIC concentration and δ^{13}C-DIC In the legend, the Z and N represent the ZCS and NJ water column respectively; number 1, 4, 7 and 10 represent January, April, July and October. Z-1 represents the variations of ZCS water column in January.

Fig. S5), the negative correlation between Δ^{34}S and environmental factors such as pH, O_2 and T further indicated that the hypoxic and reducing environment favored the BSR process and promoted S isotope fractionation. In July, with highest RWCS during the year, the great differences of T, pH and O_2 at different depths caused significant differences in SRB community. The RWCS weakened in October, and the difference of water chemistry between

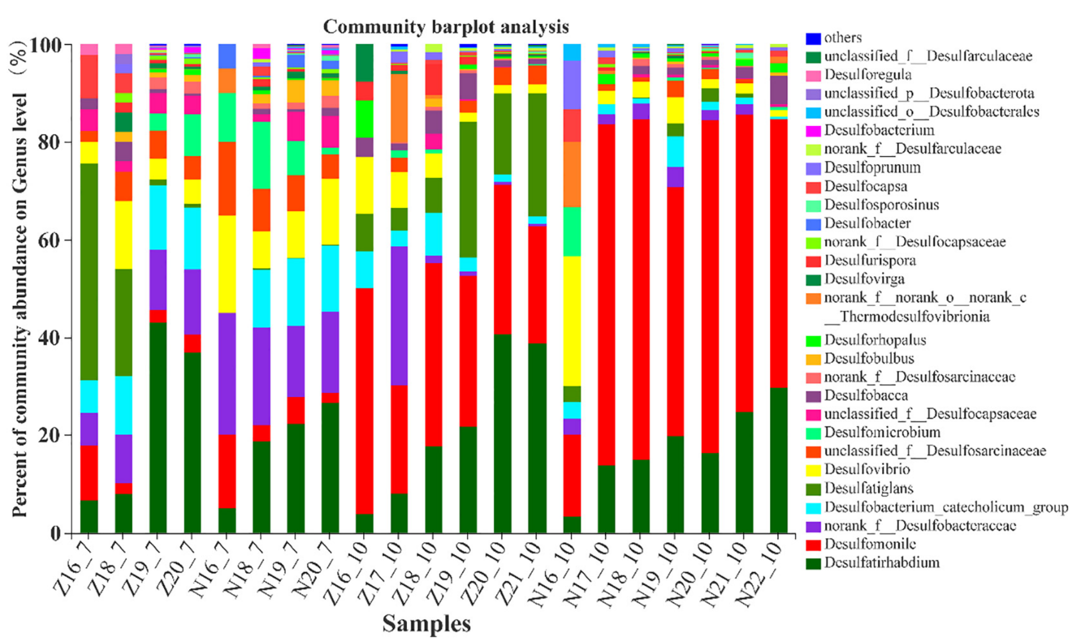

Fig. 5. Spatiotemporal variations of sulfate-reducing bacteria composition in ZCS and NJ in July and October. From the bottom to the top, the legend corresponds to the color of the bars in the barplot, the sixth and eighth bars colored in bright yellow and bright green are dominant incomplete oxidizers *Desulfovibrio* and *Desulfomicrobium* respectively. And the sample named Z16_7 originates from the ZCS water column at depth 16 m in July.

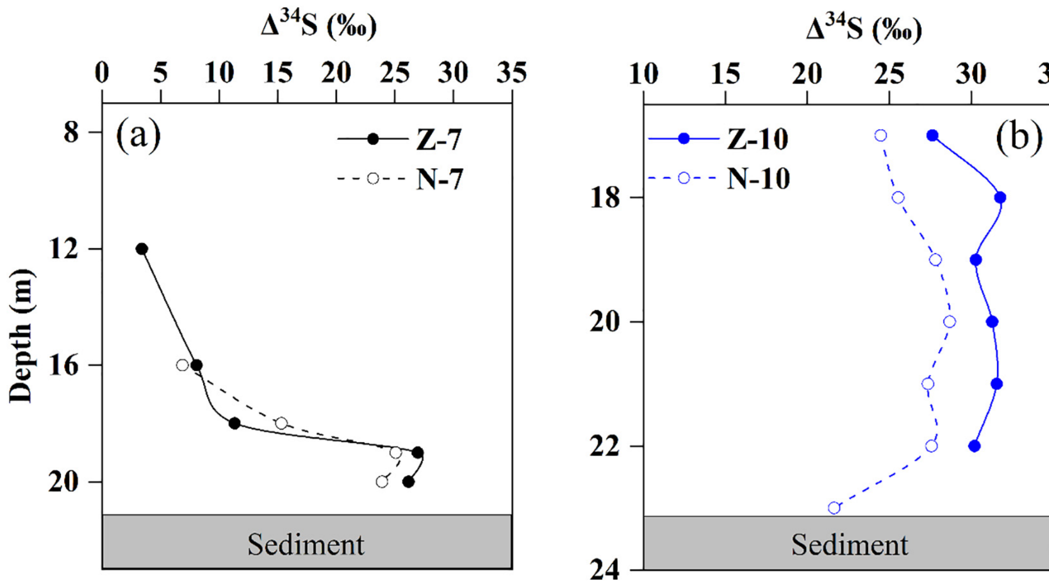

Fig. 6. Spatial and seasonal variations of S isotope difference between sulfate and sulfide ($\Delta^{34}S$).

different layers was reduced (Cui et al., 2021; Yang et al., 2020b), which was also reflected in a smaller difference of SRB composition (Fig. 5). Overall, we suggest that the composition of sulfate reducers caused the significant difference of $\Delta^{34}S$ with depth in July, while weakened RWCS in October reduced the differences in SRB diversity and caused greater but more stable S isotope fractionation in the water column.

4.3. CS coupling mechanism of during BSR

4.3.1. Co-occurrence of BSR and OC mineralization

Photosynthesis preferentially utilizes ^{12}C-DIC and leaves the residual DIC enriched in ^{13}C in the surface water, while OC mineralization increased the relative ^{13}C-DIC depletion in the bottom waters (Wang et al., 2019). The spatiotemporal variations of DIC and δ^{13}C-DIC (Fig. 4) implicated that OC mineralization proceeded in the hypoxic water in July and October. The significant increase of $\delta^{34}S\text{-}SO_4^{2-}$ and sulfide production shown in Fig. 3 signaled the widespread occurrence of BSR. Furthermore, δ^{13}C-DIC decreased concurrently with the increase of $\delta^{34}S\text{-}SO_4^{2-}$ in bottom hypoxic water in July and October (Fig. S6), suggesting the co-occurrence of sulfate reduction and OC mineralization based on Eq. (2) (Cui et al., 2020; Hosono et al., 2014).

The DIC concentration increased concurrently with the decrease of δ^{13}C-DIC (Fig. 4) with a significant correlation (*p* < *0.05*; Fig. S6), indicating the DIC production from OC mineralization was dominant (Gammons et al., 2014; Hosono et al., 2014). In the present study, the mean values of δ^{13}C-DIC and DIC concentration of samples at Station ZCS and NJ in January were set as the starting point for the OC mineralization, and the specific calculation of ΔDIC and Δ^{13}C-DIC could be defined as (Cui et al., 2020):

$$\Delta DIC = DIC_{(sample)} - DIC_{(average\ in\ January)} \tag{4}$$

$$\Delta^{13}C{-}DIC = \delta^{13}C - DIC_{(sample)} - \delta^{13}C - DIC_{(average\ in\ January)} \tag{5}$$

where the ΔDIC or Δ^{13}C-DIC represented the difference between the DIC or δ^{13}C-DIC values of water samples in other seasons and those of the average value in January. The ΔDIC showed negative correlation with Δ^{13}C-DIC both in July and October (*p* < *0.05*) (Fig. S7), revealing the ΔDIC could represent the DIC generated by OC mineralization in this study. Interestingly, ΔDIC concentration was positively correlated with the $\Delta^{34}S$ in July and Δ^{13}C-DIC was negatively correlated with the $\Delta^{34}S$ in October in the bottom hypoxic water ($p < 0.01$) (Fig. 7). The generated ΔDIC from OC mineralization would inherit the negative isotope signal from POC (δ^{13}C-POC, between −33.4 and −21.2‰) and/or DOC (δ^{13}C-

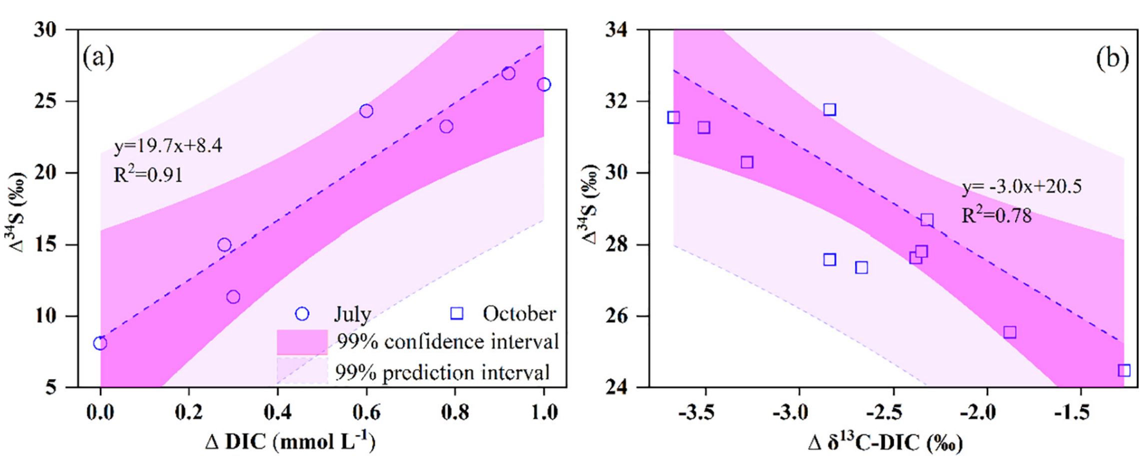

Fig. 7. Relationship between ΔDIC concentration, Δ^{13}C-DIC and $\Delta^{34}S$. The mean δ^{13}C-DIC and DIC concentration of the ZCS and NJ profile samples in January was set as the starting point, and the Δ^{13}C-DIC and ΔDIC were obtained from the difference between the samples in July (a) and October (b) and the starting point.

DOC, from −28.6 to −26.8‰), which were recently reported in other reservoirs in Guizhou Province, since they were both in karst area and influenced by human activity (Xiao et al., 2021; Yi et al., 2021). Meanwhile, the sulfide produced from BSR would be relatively depleted in ^{34}S, resulting in the remaining SO_4^{2-} relatively enriched in ^{34}S (Zerkle et al., 2010). The linear relationship between $\Delta^{34}S$ and ΔDIC or $\Delta^{13}C$-DIC reflected a tighter coupling relationship between C and S during BSR.

4.3.2. CS coupling mechanism during different periods of stratification

The ΔDIC concentrations were positively correlated with the $\Delta^{34}S$ in July, implying that the S isotope fractionation in BSR was influenced by the amount of OC that was mineralized. In contrast, the DOC concentrations were poorly correlated with DIC concentration and $\Delta^{34}S$ (Fig. S5), but the ΔDIC concentrations had positive correlation with the $\Delta^{34}S$ (Fig. 7), indicating that the OC availability rather than the OC concentration controlled the amount of OC mineralization and the S isotope fractionation (Leavitt et al., 2013). Generally, small molecules of DOC derived from the degradation of macromolecular OM are more easily used by cells to achieve electron transport and obtain energy (Detmers et al., 2001; Komada et al., 2016). Therefore, the OC availability might directly determine the amount of OC mineralization. Meanwhile, in July, the relative abundance of incomplete oxidizers, *Desulfovibrio* and *Desulfomicrobium,* were much higher (in average of 13.55% and 6.85%, respectively) than that in October (with mean value of 6.85% and 0.65%, respectively) (Fig. 8), which could have yielded relatively small S isotope fractionation and ΔDIC production (Detmers et al., 2001; Hamilton et al., 2016). The strong negative correlation between ΔDIC and proportion of incomplete-oxidizing SRB also potentially indicated the effect of OC availability on the relative composition of different SRBs in July (Fig. S8). Since different types of SRB have different preferences for organic substrates, the influence of OC availability in BSR is reflected in which organic molecules were preferred to be used by the dominant SRB_S in the study area (Muyzer and Stams, 2008). To sum up, the expectedly high OC availability due to high primary productivity in July could favor the competitive growth of complete and incomplete oxidizers of SRB, and the DIC production and the S isotope fractionation were both related to the proportion of these two types SRB involved in BSR.

The negative correlation of $\Delta^{13}C$-DIC to $\Delta^{34}S$ in October in the bottom hypoxic water suggested the generated DIC was more depleted in ^{13}C while S isotope fractionation was enlarged in BSR. In October, further development of hypoxia induced anaerobic degradation of OM and recalcitrant substances, such as lignin, being depleted in ^{13}C (Benner et al., 1987; Krüger et al., 2014), would be also degraded into smaller molecules. The newly replenished smaller molecular OC was possibly used by complete-oxidizing SRBs like *Desulfatiglans*, *Desulfomonile* that caused relatively large S isotope fractionation (Detmers et al., 2001; Hamilton et al., 2016). Since the composition of the OM varied in different season, it was likely that the anaerobic food chain and the microbial community of sulfate reducers in July and October varied as well (Detmers et al., 2001). The range of organic substrates available to these complete oxidizers was relatively wide (Sun et al., 2001). Meanwhile, the relative abundance of complete oxidizers was higher in October in comparison to July (Fig. 8). Therefore, due to the physiological characteristics of complete oxidizers among the SRB, the BSR process led to a greater S isotope fractionation in October. We conclude that the newly degraded macromolecular OM depleted in ^{13}C was utilized by the dominant complete oxidizers, resulting in the generation of ^{13}C-depleted DIC and larger S isotope fractionation in the BSR process.

Sulfate in the Aha reservoir is mainly derived from sulfide minerals and pyrite in coal, and a small percentage of atmospheric precipitation (Song

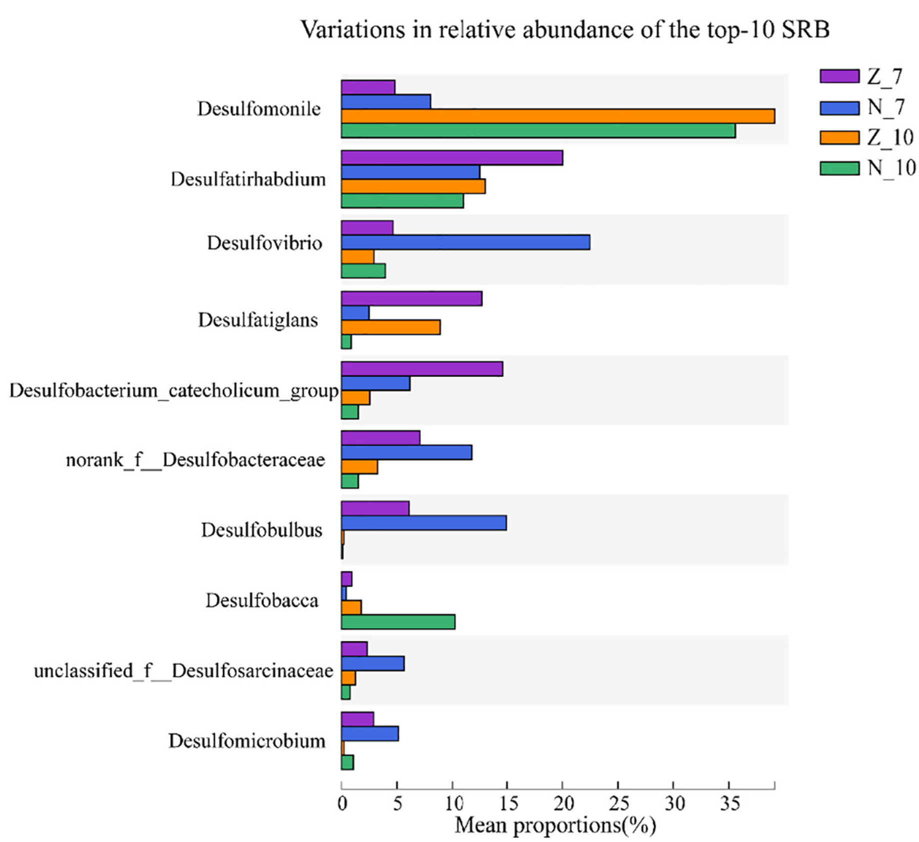

Fig. 8. Difference of the relative abundance between the top-10 sulfate-reducing bacteria in different profiles in July and October. In the legend, the Z and N represent the ZCS and NJ water column respectively; number 7 and 10 represent July and October, and Z-7 represents the variations of ZCS water column in July.

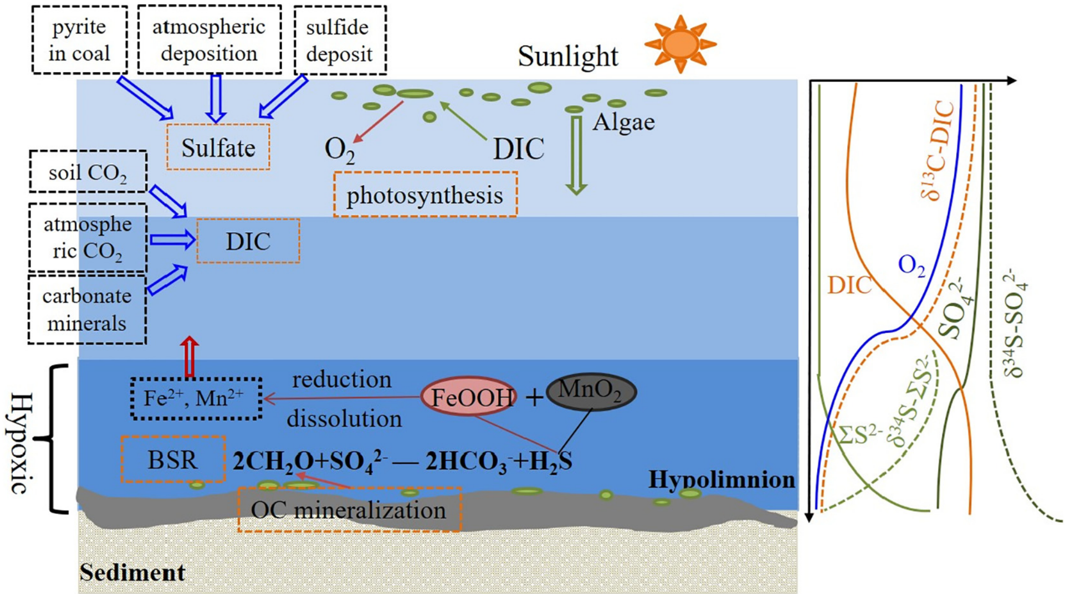

Fig. 9. Carbon and sulfur cycling influenced by thermal stratification in Aha reservoir.

et al., 2011), while DIC is mainly derived from soil CO_2, atmospheric CO_2 and carbonate minerals (Li et al., 2010). The sources of SO_4^{2-} and DIC do not vary significantly between seasons. In addition, variations in water chemistry in the water column result in seasonal thermal stratification, which finally shapes the biogeochemical cycling of C and S in the surface aerobic and bottom hypoxic water column. Of particular importance are the processes of coupled OC mineralization with sulfate reduction under high SO_4^{2-} conditions (Fig. 9). We conclude that well-defined correlations between Δ^{34}S and ΔDIC or Δ^{13}C-DIC reveal the composition and availability of OC, which might control the coupling of BSR and OC mineralization by influencing the SRB diversity. In turn, the OC mineralization coupled to sulfate reduction could affect the water quality of the bottom water and the cycling of other elements.

5. Conclusions

Thermal stratification from April to October and the hypoxia formed in the bottom water in July and October in Aha reservoir were observed in the present study. Spatially, the increase of the relative abundance of SRB with depth in the water column resulted in increasing of ΣS^{2-} with depth in summer. Seasonally, the significant decrease of SO_4^{2-} and high ΣS^{2-} in the hypolimnion in October compared to July was mainly caused by the higher degree of BSR in October. The magnitude of S isotope fractionation expressed as Δ^{34}S in BSR was influenced by the diversity of sulfate reducers. The high RWCS in July caused notable differences in water chemistry and SRB diversity with depth, which caused greater variations of Δ^{34}S with depths compared to that in October. Moreover, the concurrent decrease of δ^{13}C-DIC with δ^{34}S-SO_4^{2-} increase in hypoxic water indicated the coupling of BSR and OC mineralization. Specially, the Δ^{34}S scaled a strong positive relation with ΔDIC in July and a negative relation with Δ^{13}C-DIC in October, suggesting the composition of SRB (proportion of complete oxidizer and incomplete oxidizer) played an important role in controlling S isotope fractionation during BSR in July and October. Meanwhile, the composition and availability of OC indirectly affect the S isotope fractionation by shaping the composition of SRB community. It should be noted that further study on the isotopic and compositional variations of DOC would be needed to understand the coupling mechanisms of C and S in this and other hypoxic water bodies.

Declaration of competing interest

The authors declare that they have no known competing financial interests or personal relationships that could have appeared to influence the work reported in this paper.

Acknowledgments

We are grateful to Yingying Chen, Qingkai Li, Xiaoqing Feng, Siqi Li, Jun Zhang and Yuanbi Yi for their help in the field work and teacher Ning An and Li Lu for the test work in the lab. We are also very grateful to professor Bo Barker Jørgensen at Aarhus University for his valuable advice on the revision of the manuscript. This study was financially supported by the National Natural Science Foundation of China (U1612442), the Opening Fund of the State Key Laboratory of Environmental Geochemistry (SKLEG2021210), Tianjin Research Innovation Project for Postgraduate Students (2020YJSB060) and Public Study Abroad Program of China Scholarship Council.

Appendix A. Supplementary data

Supplementary data to this article can be found online at https://doi.org/10.1016/j.scitotenv.2022.154537.

References

Al-Raei, A.M., Bosselmann, K., Böttcher, M.E., Hespenheide, B., Tauber, F., 2009. Seasonal dynamics of microbial sulfate reduction in temperate intertidal surface sediments: controls by temperature and organic matter. Ocean Dyn. 59, 351–370.
Antler, G., Holm, S.A., Findlay, A.J., Crockford, P.W., Turchyn, A.V., Pellerin, A., 2019. Large sulfur isotope fractionation by bacterial sulfide oxidation. Sci. Adv. 5, eaaw1480.
Becker, V., Huszar, V.L.M., Naselli-Flores, L., PadisÁK, J., 2008. Phytoplankton equilibrium phases during thermal stratification in a deep subtropical reservoir. Freshw. Biol. 53 (5), 952–963. https://doi.org/10.1111/j.1365-2427.2008.01957.x.
Benner, R., Fogel, M.L., Sprague, E.K., Hodson, R.E., 1987. Depletion of 13C in lignin and its implications for stable carbon isotope studies. Nature 329, 708–710.

Borch, T., Kretzschmar, R., Kappler, A., Cappellen, P.V., Ginder-Vogel, M., Voegelin, A., et al., 2010. Biogeochemical redox processes and their impact on contaminant dynamics. Environ. Sci. Technol. 44, 15–23.

Bradley, A.S., Leavitt, W.D., Schmidt, M., Knoll, A.H., Girguis, P.R., Johnston, D.T., 2016. Patterns of sulfur isotope fractionation during microbial sulfate reduction. Geobiology 14, 91–101.

Cai, C., Li, K., Liu, D., John, C.M., Wang, D., Fu, B., et al., 2021. Anaerobic oxidation of methane by mn oxides in sulfate-poor environments. Geology 49, 761–766.

Canfield, D.E., 2001. Isotope fractionation by natural populations of sulfate-reducing bacteria. Geochim. Cosmochim. Acta 65, 1117–1124.

Cao, X., Wu, P., Zhou, S., Sun, J., Han, Z., 2018. Tracing the origin and geochemical processes of dissolved sulphate in a karst-dominated wetland catchment using stable isotope indicators. J. Hydrol. 562, 210–222.

Cui, G., Li, X.-d., Yang, M., Ding, S., Li, Q.-k., Wang, Y., et al., 2020. Insight into the mechanisms of denitrification and sulfate reduction coexistence in cascade reservoirs of the Jialing River: evidence from a multi-isotope approach. Sci. Total Environ. 749, 141682.

Cui, G., Wang, B., Xiao, J., Qiu, X.-L., Liu, C.-Q., Li, X.-D., 2021. Water column stability driving the succession of phytoplankton functional groups in karst hydroelectric reservoirs. J. Hydrol. 592, 125607.

Dalcin Martins, P., Hoyt, D.W., Bansal, S., Mills, C.T., Tfaily, M., Tangen, B.A., et al., 2017. Abundant carbon substrates drive extremely high sulfate reduction rates and methane fluxes in prairie pothole wetlands. Glob. Chang. Biol. 23, 3107–3120.

Desortová, B., 1981. Relationship between chlorophyll-α concentration and phytoplankton biomass in several reservoirs in czechoslovakia. Int. Rev. Gesamten Hydrobiol. Hydrogr. 66, 153–169.

Detmers, J., Brüchert, V., Habicht, K.S., Kuever, J., 2001. Diversity of sulfur isotope fractionations by sulfate-reducing prokaryotes. Appl. Environ. Microbiol. 67, 888.

Diaz, R.J., Rosenberg, R., 2008. Spreading dead zones and consequences for marine ecosystems. Science 321, 926.

Ding, S., Wang, Y., Yang, M., Shi, R., Ma, T., Cui, G., et al., 2022. Distribution and speciation of arsenic in seasonally stratified reservoirs: implications for biotransformation mechanisms governing interannual variability. Sci. Total Environ. 806, 150925.

Fahrner, S., Radke, M., Karger, D., Blodau, C., 2008. Organic matter mineralisation in the hypolimnion of an eutrophic maar lake. Aquat. Sci. 70, 225–237.

Feng, X., Bai, W., Shang, L., He, T., Qiu, G., Yan, H., 2011. Mercury speciation and distribution in Aha Reservoir which was contaminated by coal mining activities in Guiyang, Guizhou, China. Appl. Geochem. 26, 213–221.

Findlay, A.J., Boyko, V., Pellerin, A., Avetisyan, K., Guo, Q., Yang, X., et al., 2019. Sulfide oxidation affects the preservation of sulfur isotope signals. Geology 47, 739–743.

Gammons, C.H., Henne, W., Poulson, S.R., Parker, S.R., Johnston, T.B., Dore, J.E., et al., 2014. Stable isotopes track biogeochemical processes under seasonal ice cover in a shallow, productive lake. Biogeochemistry 120, 359–379.

Geng, L., Savarino, J., Savarino, C.A., Caillon, N., Cartigny, P., Hattori, S., et al., 2018. A simple and reliable method reducing sulfate to sulfide for multiple sulfur isotope analysis. Rapid Commun. Mass Spectrom. 32, 333–341.

Glombitza, C., Stockhecke, M., Schubert, C.J., Vetter, A., Kallmeyer, J., 2013. Sulfate reduction controlled by organic matter availability in deep sediment cores from the saline, alkaline Lake Van (Eastern Anatolia, Turkey). Front. Microbiol. 4 209-209.

Hamilton, T.L., Bovee, R.J., Sattin, S.R., Mohr, W., Gilhooly, W.P., Lyons, T.W., et al., 2016. Carbon and sulfur cycling below the chemocline in a meromictic Lake and the identification of a novel taxonomic lineage in the FCB superphylum, candidatus aegiribacteria. Front. Microbiol. 7.

Han, M., Li, Q., Chen, H., Xiao, J., Jiang, F., 2018. Spatial and temporal variations in cyanobacteria and microcystins in aha reservoir, Southwest China. J. Oceanol. Limnol. 36, 1126–1131.

Holmer, M., Storkholm, P., 2001. Sulphate reduction and Sulphur cycling in lake sediments: a review. Freshw. Biol. 46, 431–451.

Hosono, T., Tokunaga, T., Tsushima, A., Shimada, J., 2014. Combined use of delta(13)C, delta (15)N, and delta(34)S tracers to study anaerobic bacterial processes in groundwater flow systems. Water Res. 54, 284–296.

Jørgensen, B.B., 1982. Mineralization of organic matter in the sea bed—the role of sulphate reduction. Nature 296, 643–645.

Jørgensen, B.B., Findlay, A.J., Pellerin, A., 2019. The biogeochemical sulfur cycle of marine sediments. Front. Microbiol. 10, 849.

Kasprzak, P., Padisák, J., Koschel, R., Krienitz, L., Gervais, F., 2008. Chlorophyll a concentration across a trophic gradient of lakes: an estimator of phytoplankton biomass? Limnologica 38, 327–338.

Kleikemper, J., Schroth, M.H., Bernasconi, S.M., Brunner, B., Zeyer, J., 2004. Sulfur isotope fractionation during growth of sulfate-reducing bacteria on various carbon sources. Geochim. Cosmochim. Acta 68, 4891–4904.

Knossow, N., Blonder, B., Eckert, W., Turchyn, A.V., Antler, G., Kamyshny Jr., A., 2015. Annual sulfur cycle in a warm monomictic lake with sub-millimolar sulfate concentrations. Geochem. Trans. 16, 7.

Komada, T., Burdige, D.J., Li, H.-L., Magen, C., Chanton, J.P., Cada, A.K., 2016. Organic matter cycling across the sulfate-methane transition zone of the Santa Barbara Basin, California Borderland. Geochim. Cosmochim. Acta 176, 259–278.

Krüger, J.P., Leifeld, J., Alewell, C., 2014. Degradation changes stable carbon isotope depth profiles in palsa peatlands. Biogeosciences 11, 3369–3380.

Kushkevych, I., Dordević, D., Vítězová, M., 2019. Analysis of pH dose-dependent growth of sulfate-reducing bacteria. Open Med. 14, 66–74.

Kwon, M.J., O'Loughlin, E.J., Boyanov, M.I., Brulc, J.M., Johnston, E.R., Kemner, K.M., et al., 2016. Impact of organic carbon electron donors on microbial community development under iron- and sulfate-reducing conditions. PLoS ONE 11, e0146689.

Lawson, R., Anderson, M.A., 2007. Stratification and mixing in Lake Elsinore, California: an assessment of axial flow pumps for improving water quality in a shallow eutrophic lake. Water Res. 41, 4457–4467.

Leavitt, W.D., Halevy, I., Bradley, A.S., Johnston, D.T., 2013. Influence of sulfate reduction rates on the phanerozoic sulfur isotope record. Proc. Natl. Acad. Sci. U. S. A. 110, 11244–11249.

Lewicka-Szczebak, D., Trojanowska, A., Górka, M., Jędrysek, M.-O., 2008. Sulphur isotope mass balance of dissolved sulphate ion in a freshwater dam reservoir. Environ. Chem. Lett. 6, 169–173.

Li, S.-L., Liu, C.-Q., Li, J., Lang, Y.-C., Ding, H., Li, L., 2010. Geochemistry of dissolved inorganic carbon and carbonate weathering in a small typical karstic catchment of Southwest China: isotopic and chemical constraints. Chem. Geol. 277, 301–309.

Li, X.-D., Liu, C.-Q., Liu, X.-L., Bao, L.-R., 2011. Identification of dissolved sulfate sources and the role of sulfuric acid in carbonate weathering using dual-isotopic data from the Jialing River, Southwest China. J. Asian Earth Sci. 42, 370–380.

Li, X., Zhang, S., Yang, M., 2014. Accumulation and risk assessment of heavy metals in dust in main living areas of Guiyang City, Southwest China. Chin. J. Geochem. 33, 272–276.

Li, S.-L., Xu, S., Wang, T.-J., Yue, F.-J., Peng, T., Zhong, J., et al., 2020. Effects of agricultural activities coupled with karst structures on riverine biogeochemical cycles and environmental quality in the karst region. Agric. Ecosyst. Environ. 303, 107120.

Luek, J.L., Thompson, K.E., Larsen, R.K., Heyes, A., Gonsior, M., 2017. Sulfate reduction in sediments produces high levels of chromophoric dissolved organic matter. Sci. Rep. 7, 8829.

Mori, F., Umezawa, Y., Kondo, R., Wada, M., 2018. Dynamics of sulfate-reducing bacteria community structure in surface sediment of a seasonally hypoxic Enclosed Bay. Microbes Environ. 33, 378–384.

Muyzer, G., Stams, A.J.M., 2008. The ecology and biotechnology of sulphate-reducing bacteria. Nat. Rev. Microbiol. 6, 441–454.

Mylon, S.E., Benoit, G., 2001. Subnanomolar detection of acid-labile sulfides by the classical methylene blue method coupled to HPLC. Environ. Sci. Technol. 35, 4544–4548.

Niggemann, J., Ferdelman, T.G., Lomstein, B.A., Kallmeyer, J., Schubert, C.J., 2007. How depositional conditions control input, composition, and degradation of organic matter in sediments from the chilean coastal upwelling region. Geochim. Cosmochim. Acta 71, 1513–1527.

Robador, A., Brüchert, V., Jørgensen, B.B., 2009. The impact of temperature change on the activity and community composition of sulfate-reducing bacteria in arctic versus temperate marine sediments. Environ. Microbiol. 11, 1692–1703.

Song, L., Liu, C., Wang, Z., Teng, Y., Wang, J., Liang, L., et al., 2011. Seasonal variations in sulfur isotopic composition of dissolved SO42− in the aha Lake, Guiyang and their implications. Chin. J. Geochem. 30, 444–452.

Stam, M.C., Mason, P.R.D., Pallud, C., Van Cappellen, P., 2010. Sulfate reducing activity and sulfur isotope fractionation by natural microbial communities in sediments of a hypersaline soda Lake (Mono lake, California). Chem. Geol. 278, 23–30.

Sun, B., Cole, J.R., Tiedje, J.M., 2001. Desulfomonile limimaris sp. nov., an anaerobic dehalogenating bacterium from marine sediments. Int. J. Syst. Evol. Microbiol. 51, 365–371.

Sun, W., Xiao, T., Sun, M., Dong, Y., Ning, Z., Xiao, E., et al., 2015. Diversity of the sediment microbial Community in the aha Watershed (Southwest China) in response to acid mine drainage pollution gradients. Appl. Environ. Microbiol. 81, 4874–4884.

Tong, J., Zhang, H., Yang, D., Zhang, Y., Xiong, B., Jiang, L., 2018. Illumina sequencing analysis of the ruminal microbiota in high-yield and low-yield lactating dairy cows. PLOS ONE 13, e0198225.

Wang, F., 2020. Impact of a large sub-tropical reservoir on the cycling of nutrients in a river. Water Res. 186, 116363.

Wang, F., Yu, Y., Liu, C., Wang, B., Wang, Y., Guan, J., et al., 2010. Dissolved silicate retention and transport in cascade reservoirs in karst area, Southwest China. Sci. Total Environ. 408, 1667–1675.

Wang, W., Li, S.-L., Zhong, J., Li, C., Yi, Y., Chen, S., et al., 2019. Understanding transport and transformation of dissolved inorganic carbon (DIC) in the reservoir system using δ13CDIC and water chemistry. J. Hydrol. 574, 193–201.

Wasmund, K., Mußmann, M., Loy, A., 2017. The life sulfuric: microbial ecology of sulfur cycling in marine sediments. Environ. Microbiol. Rep. 9, 323–344.

Winton, R.S., Calamita, E., Wehrli, B., 2019. Reviews and syntheses: dams, water quality and tropical reservoir stratification. Biogeosciences 16, 1657–1671.

Xiao, J., Wang, B., Qiu, X.-L., Yang, M., Liu, C.-Q., 2021. Interaction between carbon cycling and phytoplankton community succession in hydropower reservoirs: evidence from stable carbon isotope analysis. Sci. Total Environ. 774, 145141.

Xing, P., Tao, Y., Luo, J., Wang, L., Li, B., Li, H., et al., 2019. Stratification of microbiomes during the holomictic period of Lake fuxian, an alpine monomictic lake. Limnol. Oceanogr. 65.

Yang, M., Li, X.-D., Huang, J., Ding, S., Cui, G., Liu, C.-Q., et al., 2020a. Damming effects on river sulfur cycle in karst area: a case study of the wujiang cascade reservoirs. Agric. Ecosyst. Environ. 294, 106857.

Yang, M., Shi, J., Wang, B., Xiao, J., Li, W., Liu, C.-Q., 2020b. Control of hydraulic load on bacterioplankton diversity in cascade hydropower Reservoirs, Southwest China. Microb. Ecol. 80, 537–545.

Yi, Y., Zhong, J., Bao, H., Mostofa, K.M.G., Xu, S., Xiao, H.-Y., et al., 2021. The impacts of reservoirs on the sources and transport of riverine organic carbon in the karst area: a multi-tracer study. Water Res. 194, 116933.

Zak, D., Hupfer, M., Cabezas, A., Jurasinski, G., Audet, J., Kleeberg, A., et al., 2021. Sulphate in freshwater ecosystems: a review of sources, biogeochemical cycles, ecotoxicological effects and bioremediation. Earth Sci. Rev. 212, 103446.

Zerkle, A.L., Kamyshny, A., Kump, L.R., Farquhar, J., Oduro, H., Arthur, M.A., 2010. Sulfur cycling in a stratified euxinic lake with moderately high sulfate: constraints from quadruple S isotopes. Geochim. Cosmochim. Acta 74, 4953–4970.

Zhang, Y., Wu, Z., Liu, M., He, J., Shi, K., Zhou, Y., et al., 2015. Dissolved oxygen stratification and response to thermal structure and long-term climate change in a large and deep subtropical reservoir (Lake qiandaohu, China). Water Res. 75, 249–258.

Zhang, Y., Wang, X., Zhen, Y., Mi, T., He, H., Yu, Z., 2017. Microbial diversity and community structure of sulfate-reducing and sulfur-oxidizing bacteria in sediment cores from the East China Sea. Front. Microbiol. 8 2133-2133.

Zhang, J., Ma, T., Yan, Y., Xie, X., Abass, O.K., Liu, C., et al., 2018. Effects of fe-S-as coupled redox processes on arsenic mobilization in shallow aquifers of Datong Basin, northern China. Environ. Pollut. 237, 28–38.

Zhang, X., Ding, S., Lv, H., Cui, G., Yang, M., Wang, Y., et al., 2022. Microbial controls on heavy metals and nutrients simultaneous release in a seasonally stratified reservoir. Environ. Sci. Pollut. Res. 29, 1937–1948.